Aperture Efficiency and Astigmatism Measurements at 87-110 GHz

M. Visús, P. de Vicente, A. Pérez
V. Bujarrabal, A. Díaz-Pulido

Informe Técnico IT-CDT 2012-20

Revision history

Version	Date	Author	Updates
1.0	25-07-2012	P. de Vicente	First version

Contents

1 Introduction

The need for the optimization of the subreflector position at 86 GHz was clear after de Vicente (2012) and López-Pérez (2012), as well as the implementation of another pointing model after that. This report shows the results of the analysis done in order to reduce the lateral defocussing, to improve the pointing accuracy and estimate the current values for the gain and the aperture efficiency.

Observations in the continuum were performed between March and May 2012 at 22 and 87 GHz.

2 Lateral defocussing

Double pointing scans at different elevations were made towards Mars, Venus and Saturn at 87 GHz between March 17th and May 14th 2012 using 7 different positions of the subreflector along axis X and Y. For each set of scans, the pointing drift that maximizes the intensity of the main beam while minimizing the intensity of the secondary lobe was found and the best focus fit has been estimated.

Figure 1 shows the dependency of the focus along Y axis as a function of elevation. The lack of bright sources with declinations close to the latitude prevented having data above 70 degrees elevation. According to the figure the subreflector should be shifted upwards by 5 mm at low elevations, and downwards by 5 mm at higher elevations.

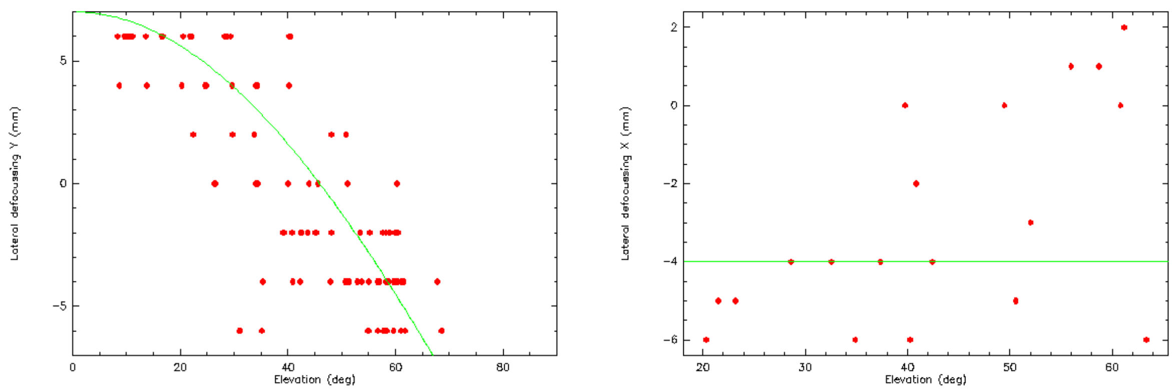

Figure 1: *Lateral defocussing for the Y and X axis versus elevation: the best fit for each case is shown (green line).*

We have fitted a curve with a cosine dependency on elevation. The final Y-axis correction to be applied is

$$\delta Y = -16 + 23\,\cos(Elevation) \tag{1}$$

Results for the X axis were less conclusive: a trend is observed but the dispersion at high elevations was so wide that no final correction should be done before new observations are made, so a -4 mm constant correction was applied, following the expected behavior of the subreflector with the elevation (de Vicente, 2008).

This new lateral focus correction was implemented and OTF maps of Mars and Saturn were performed during night time to check that the coma lobe reported by de Vicente (2012) no longer appears.

Figures 2 and 3 show that no coma lobe is present, so the bulk of the lateral defocussing was corrected. One problem that arises from those observations is that not only the main beam is broader than expected from the theoretical calculations (López-Pérez 2012) but it is also asymmetric which seems to imply that the antenna suffers from astigmatism. This problem will be discussed later.

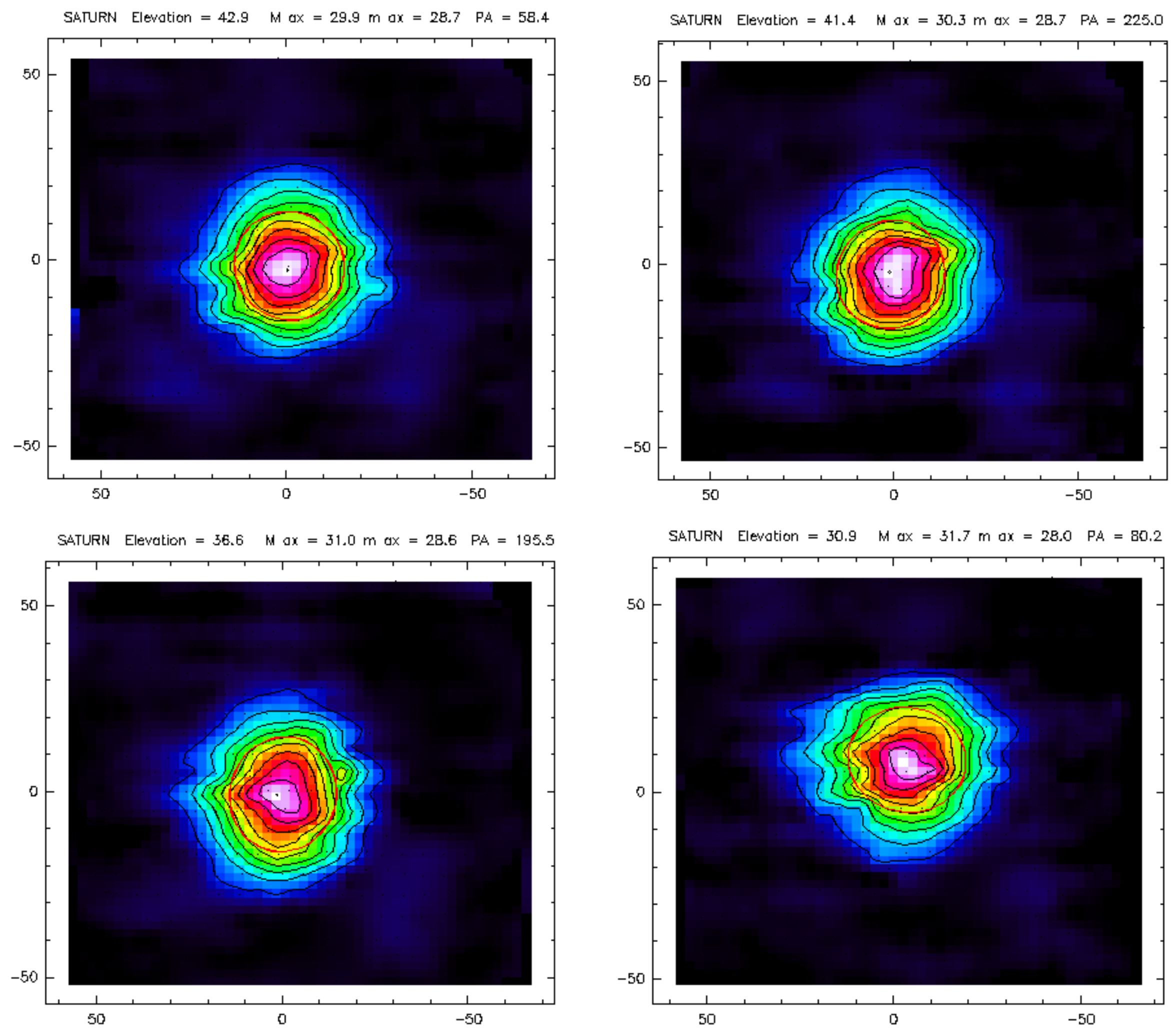

Figure 2: *Maps on Saturn after implemening the new Y focus model. From left to right an from top to bottom, the elevation of each image is 42.9, 41.4, 36.6 and 30.9 degrees*

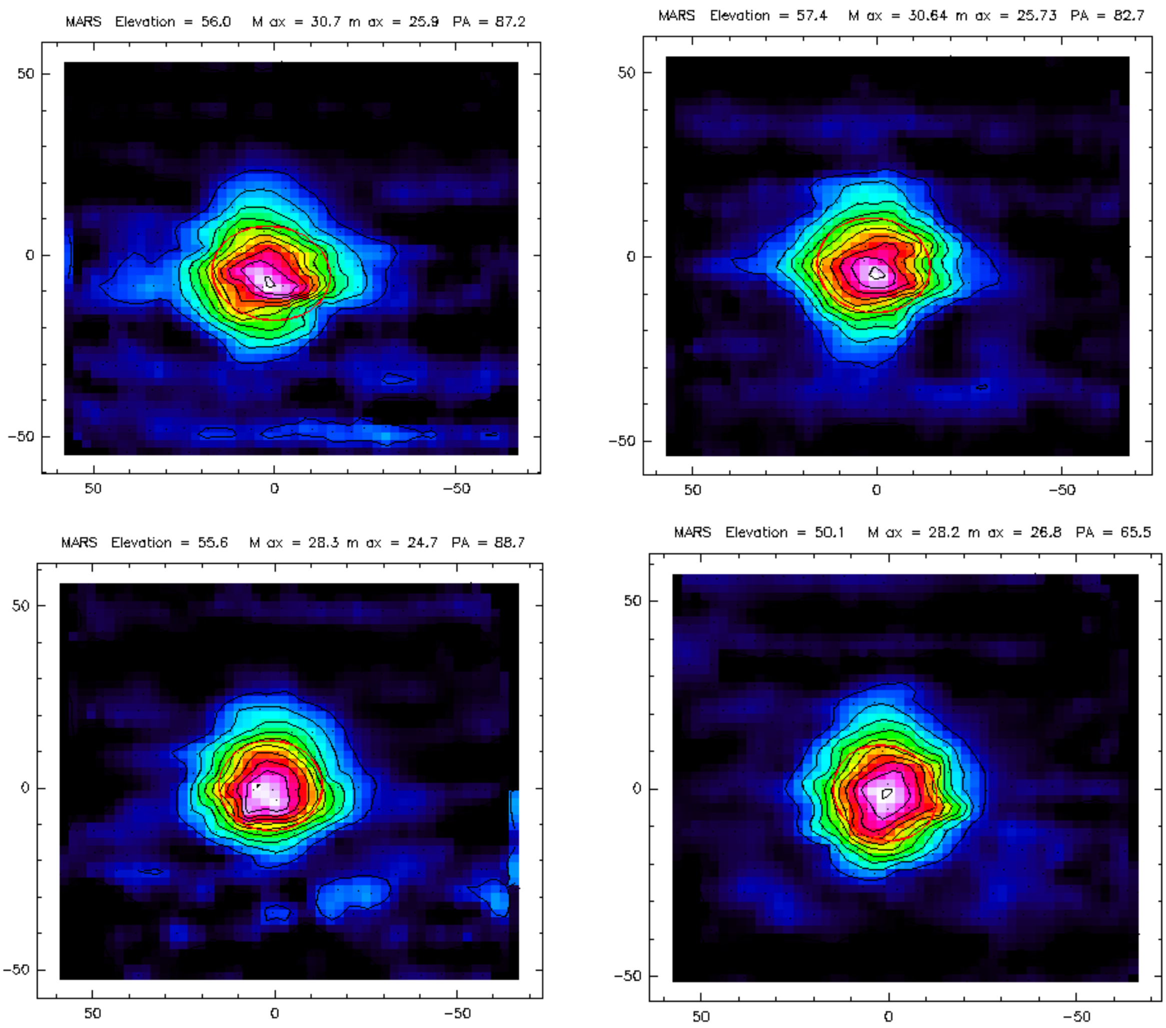

Figure 3: *Maps on Mars after implemening the new Y focus model. From left to right and from top to bottom, the elevation of each image is 56.0, 57.4, 55.6 and 50.1 degrees*

3 Pointing Model at 22GHz

A change of the focus pointing model along the X and Y axis requires a new pointing model. Ideally it would be necessary to get this pointing model al 87 GHz but the lack of bright sources (i.e. enough sources to cover the whole sky with a suitable temperature to reach a good S/N ratio) prevented it. The pointing session was done at 22 GHz after modifying the focus at this frequency. The model was computed and implemented at both frequencies (87 and 22 GHz), relying on the fact that the optical paths for the 22 and 87 GHz receivers are almost the same (M1, M2, M3, M4' and M6) except for 3 mirrors that are in the optical path of the 87 GHz receiver but not in the 22 GHz one. This has been the procedure followed previously and we believe it is a fairly good approximation.

Observations were done in May 2012 for J0319+415, J0423-013, J0437+296, J1230+123, Venus, J1229+020, J1337-129, DR21 and J1924-292.

The pointing parameters (de Vicente and Barcia, 2007) were calculated using the "OAN 40m Pointing Model" application (Alonso Albi et al. 2010) and implemented. Observations at 87 GHz were done later to check the validity of the model. Pointing errors were less than 10% of the beamwidth in all cases.

4 Gain and Aperture efficiency

After the improvements in the pointing accuracy and the reduction of the lateral defocussing, OTF maps of Mars and Saturn were done for elevations between 31 and 57 degrees using the best axial focus position for each map. The aperture efficiency was calculated for each image using

$$\eta_a = 2,197 \frac{C_s T_a'[K]}{S_f[Jy]} \tag{2}$$

with

$$C_s = \frac{x^2}{1 - e^{(-x^2)}} \tag{3}$$

where x for a disk source is

$$x = \frac{\theta_s['']}{1.2\,\theta_t['']} \tag{4}$$

θ_s is the source size and θ_t the HPBW of the antenna (see de Vicente 2012 and Baars 2007 for a complete explanation). The flux and sizes for Mars and Saturn are shown in table 1. Those observations were done without the polarizer, in an attempt to reduce the sources of systematic errors, so we compare them with the theoretical aperture efficiency without polarizer.

Source	Size [”]	Flux) [Jy]
MARS	8.1	55.44
SATURN	17.4	185.77

Table 1: *Flux and sizes for Mars and Saturn during the observation dates*

Source	Elevation [deg]	T'_a [K]	Aperture Efficiency
MARS	56.00	3.2	0.1307
	57.40	3.3	0.1354
	55.55	3.5	0.1431
	50.08	3.5	0.1439
SATURN	42.85	11.4	0.1688
	41.40	11.0	0.1626
	36.55	11.6	0.1714
	30.85	11.9	0.1760

Table 2: *Aperture efficiency at 3 mm. Ta’ is the corrected antenna temperature times the forward efficiency.*

According to López-Pérez (2012) and based on an RMS error of $\sim$ 190 μm for the primary reflector and an estimation on the surface error of the rest of the mirrors, the aperture efficiency for the 40 m radiotelescope at 3 mm without the circular polarizer should be 36%. If there is a lateral defocussing he computes an efficiency drop to 29%. The defocussing was estimated from the widening of the observed beams while pointing which he attributes to this effect. Both values are far away from the efficiency (0.14 to 0.17) that we estimate here. Even the efficiency estimated by de Vicente (2012), around 20% at 45 degree differs significantly from these values.

Figure 4 displays the aperture efficiency as function of elevation for two sets of data: the red dots show the aperture efficiency for March and the green dots stand for May. It is clear that there has been a decrease of the efficiency. As we will see latter the main hypothesis is that the antenna suffers seasonal deformations associated to the environmental temperature that modify the structure and hence the efficiency. The temperature oscillation between day and night is about 10°C in March, with maximum temperatures of 15°C, while in May, the daily oscillation spans 15°C and peaks over 30°C. The temperature would be the main cause for the degradation of the results.

We have also investigated the dependence of antenna temperature as a function of axial defocussing (along the Z axis). We did some pointing drifts along azimuth and elevation. Figure 6 shows the results of observations towards Mars and Saturn. The focus was changed two wavelengths, from -3 mm to 3 mm in steps of 1 mm.

According to Baars (2007) the antenna temperature should drop 90% with an axial defocussing of 1 wavelength. However, figure 6 shows that the intensity drops around 40% with 1

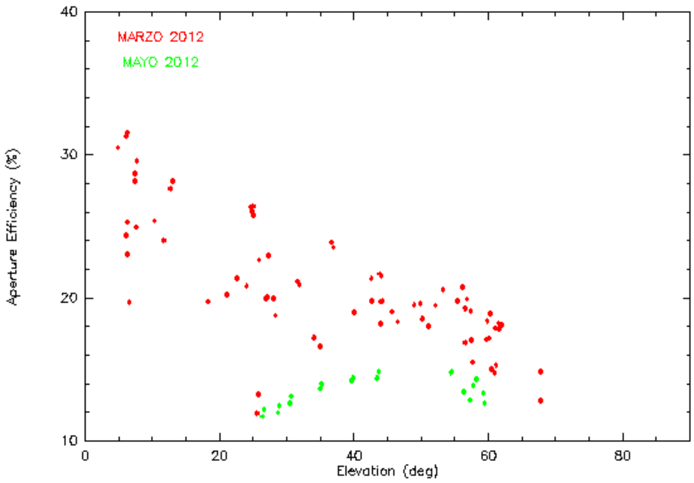

Figure 4: *Aperture efficiency as a function of elevation for two different observation periods. It is clear that the efficiency decreases with elevation, and it is considerably lower for the latest observations.*

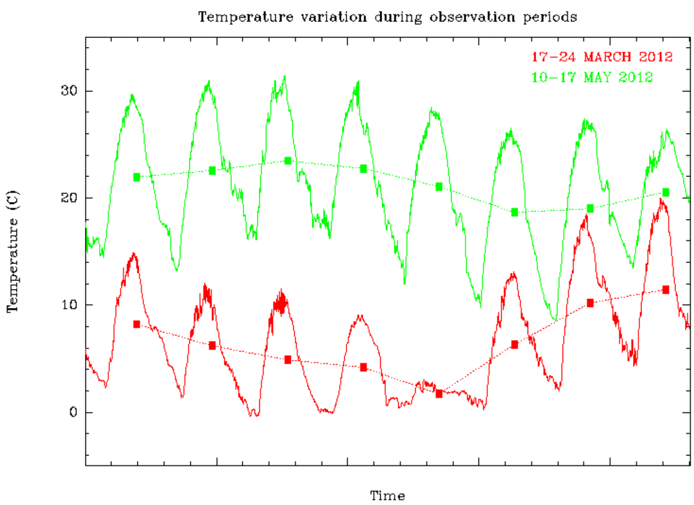

Figure 5: *Weekly temperature for the observation periods (March and May) reported here. Red and green squares indicate the daily mean temperature for March and May, respectively.*

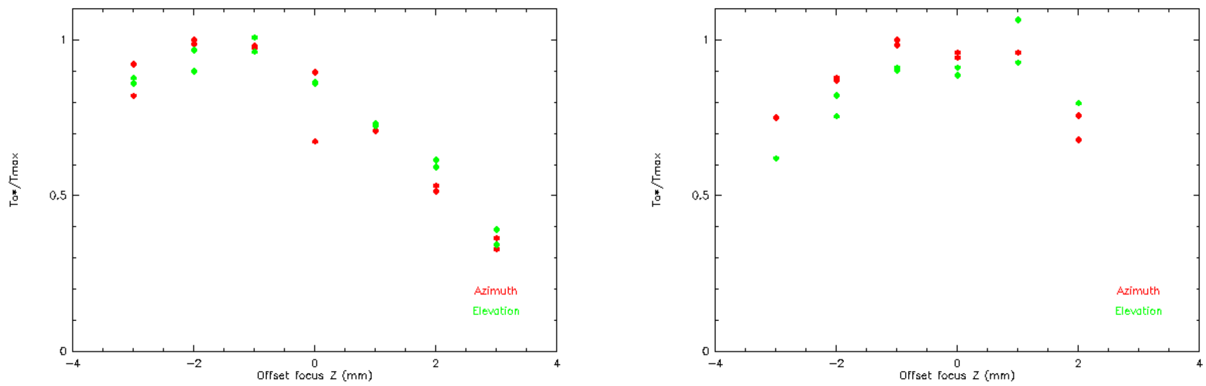

Figure 6: *Normalized Ta* curve for Mars (left) and Saturn (right) as a function of axial focus offset*

wavelength defocussing. The most probable cause is that the subreflector is not in its optimum position. Furthermore probably the current configuration of the antenna (main reflector and rest of mirrors) does not have a well defined focus, but a spread area where the intensity drops slightly when the focus changes.

The decrease of the efficiency and the low steepness of the gain as a function of axial focus points towards a large scale deformation in the antenna during spring-summer.

5 OTF Maps. Astigmatism

We have investigated the beam shape from maps towards Saturn and Mars. This was achieved by fitting 2D Gaussian fits and deconvolving later. The deconvolved beams were calculated assuming that both sources behave as disks:

$$\theta_b = \sqrt{{\theta_{conv}}^2 - \frac{ln2}{2}{\theta_{source}}^2} \tag{5}$$

where θ_{source} it the source size, θ_{conv} the measured HPBW and θ_b is the real telescope beamwidth. Results are shown in table 3

The theoretical HPBW is $\sim$ 18" (de Vicente 2012, López-Pérez 2012), whereas results compiled in table 3 show that the beam is asymmetrical and ranges between $25''$ to $32''$. This behavior is compatible with astigmatism in the primary reflector. However holography in December 2011 and January 2012 discarded the presence of astigmatism. Two main conclusions can be drawn from this fact: either the main reflector has changed since then (with a progressive deviation from the best parabolic surface as would suggest the difference between data separated two month in time), or the subreflector suffers astigmatism. The latter hypothesis is rather implausible, since it was carefully measured after built and it is expected to have low level deformations.

In order to check astigmatism, maps for some sources at different elevations and focus positions should be performed but this is a time consuming task. Provided the 3 mm receiver

Source	Elevation [deg]	Major Axis [”]	Minor Axis [”]	Position Angle [deg]
MARS	56.00	31.99	25.57	87.21
	57.40	30.26	25.30	82.80
	55.55	27.95	24.26	88.63
	50.08	27.74	26.39	66.32
SATURN	42.85	28.07	26.87	58.40
	41.40	28.38	26.63	44.85
	36.55	29.23	29.68	15.08
	30.85	29.98	26.08	80.26

Table 3: *Major and minor axes length from the fitting procedure after deconvolution*

remains cold only for a limited ammount of time and that spring-summer season is not the best season to do observational tests, we performed double pointing scans at different elevations and focus positions to check if there is an opposite broadening in orthogonal directions at one side of the best focus and at the other, as predicted by Davies (1970).

Pointing drifts were performed towards planet Mars for an elevation range between 40 and 58 degrees. Results are summarized in figure 7, where the width of the deconvolved beams along azimuth and elevation axis for different positions of the subreflector along the Z axis are shown. It can be seen that when the beam width is minimum in the azimuth drift (ΔZ = -1mm), it is maximum in elevation. And the opposite is also true: beamwidth is minimum in elevation drifts when ΔZ = 5mm and maximum for the azimuth drift at that position.

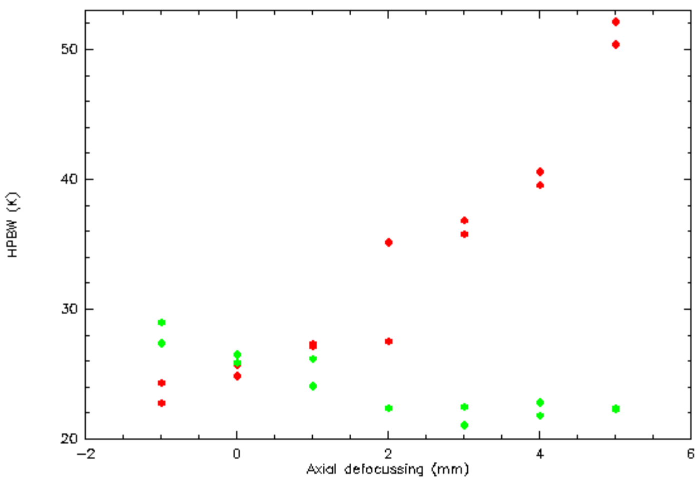

Figure 7: *Beamwidth broadening versus axial defocussing for an elevation between 40° and 58° on planet Mars. Red dots show the beamwidth along the azimuth direcction and green dots, along elevation.*

According to Greve et al. (1994) it is possible to estimate the astigmatism parameter using cross scans if the azimuth and elevation directions correspond with the principal axes of the astigmatism using point-like or extended sources alike. The dimensionless astigmatism parameter, α', is related with the geometrical amplitude of the wavefront deformation α through the expresion $\alpha' = 2\pi\alpha/\lambda$. Let $A(z/\lambda)$ be the ellipticity:

$$A(z/\lambda) = \frac{\theta_{az}}{\theta_{el}} \tag{6}$$

where θ_{az} and θ_{el} are the beamwidth along the azimuth and elevation directions, z is the axial defocussing and λ, the observing wavelength.

In a non-astigmatic telescope $A(z/\lambda) = 1$, provided $|z/\lambda| < 1$. If one represents the ellipticity as a function of axial defocus (in wavelength units) it is possible to fit a straight line with a slope and a constant term:

$$A(z/\lambda) = e_0 + S\frac{z}{\lambda} \tag{7}$$

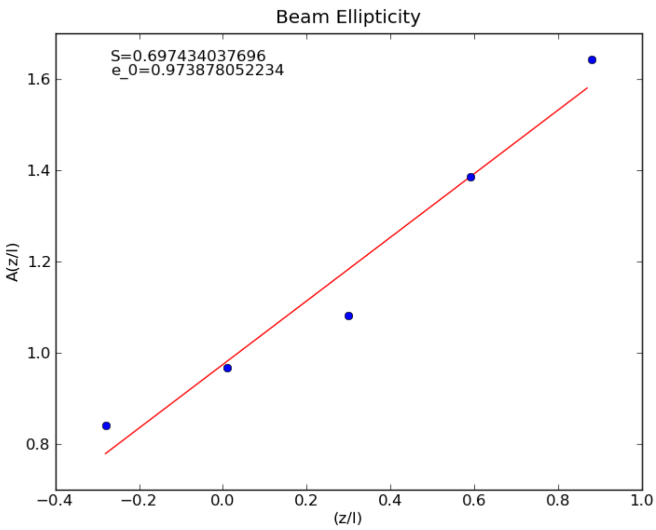

Figure 8: *Ellipticity as a function of axial defocus in wavelengths for one set of pointing drifts of Mars performed on May. In this case the slope is 0.7 and* e_0 *is 0.97. The same linear fitting was made for every set of scans.*

For point-like and extended sources, there is a unique relation between S and α' through the beam filling factor, $\beta = \theta_{source}/\theta_{tel}$, being θ_{tel} the theoretical HPBW at the best axial focus. This relation for the 40m radiotelescope is shown in figure 9 and it depends on the radiooptical parameters of the antenna. This diagnostic diagram was computed following the procedure described in Greve et al. (1994) (López-Pérez 2012, in preparation) and it can be used for a large range of wavelengths. If the considered source subtends a large fraction of the beam

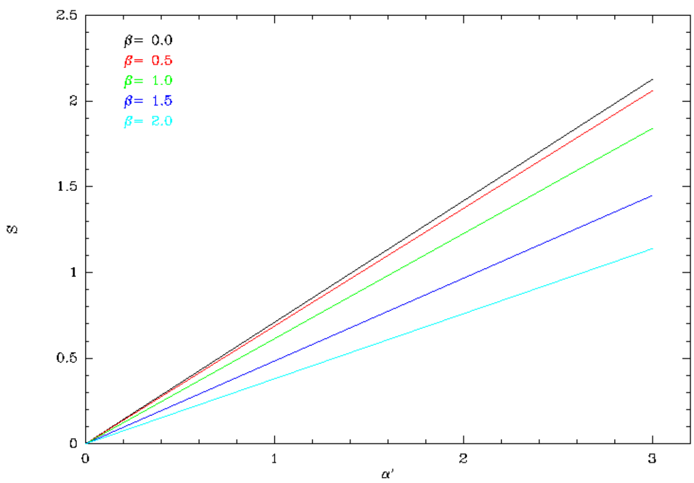

Figure 9: *Diagnostic diagram which relates S, the slope previously introduced, with the astigmatism parameter α'. Each line depends on the beam filling factor β.*

Observation Date	Elevation [deg]	β	S	α'	α [mm]	Frequency [GHz]
MARCH	42.1	0.6	0.18	0.18	0.10	85.69
MAY	49.0	0.4	0.70	1.01	0.56	86.40
AUGUST	41.3	0.0	0.56	0.78	1.67	22.24
	49.9	0.0	0.47	0.67	1.44	22.24
	49.7	0.0	0.56	0.78	1.67	22.24
	41.1	0.0	0.55	0.77	1.65	22.24
	48.7	0.0	0.23	0.32	0.69	22.24
	40.8	0.0	0.33	0.47	1.01	22.24
	49.3	0.0	0.49	0.69	1.48	22.24
	40.5	0.0	0.55	0.77	1.65	22.24
SEPTEMBER	40.0	0.7	0.59	0.91	0.50	86.24

Table 4: *Astigmatism estimation from observational data: the observational parameters are β and S, α' is estimated using the diagnostic diagram and α is calculated from it for each frequency.*

(β > 0), the astigmatism parameter is larger than for point-like sources. Table 4 shows the astigmatism parameter obtained with the diagnostic diagram for different observations.

Figure 10 shows the surface deformation as a function of environment temperature for data obtained from March to September. Since we lack 3 mm observations in summer we have also included observations at 22 GHz. The main reflector deformation has increased since March and it shows a strong dependence on the temperature, corroborating the idea of the antenna suffering a seasonal deformation.

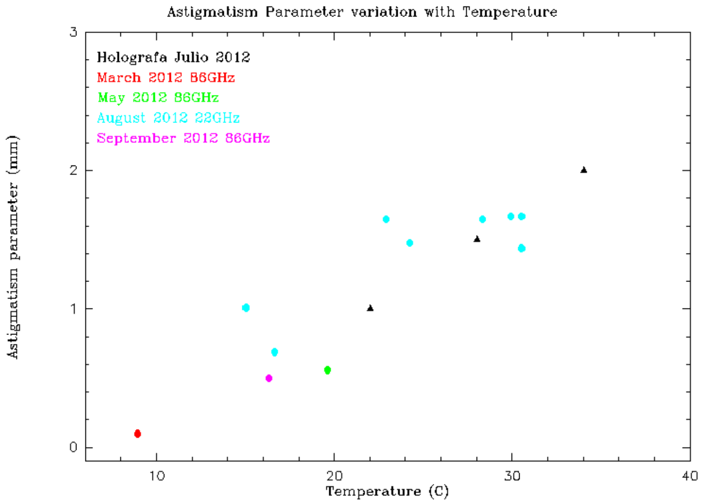

Figure 10: *Surface deformation (in mm) due to astigmatism as a function of temperature for different months. August are 22 GHz observations and March, May and September 3 mm observations.*

The influence of astigmatism over the antenna performance at 87 GHz is shown in figure 11. The aperture efficiency decreased $\sim 30\%$ between March and May, for an elevation between 46 and 49 degrees at 87 GHz and started to increase again in September when the temperatures are lower. It is not clear, however, if the surface accuracy will return to the value achieved after last winter holography. In addition, it is not possible to quantify the efficiency loss due to astigmatic deformation alone: the high temperature and its wide variation from day to nightime affect the main surface rms. Everything so far seems to indicate that observations at high frequencies during summer and even at daytime during spring/autumn are highly inadvisable.

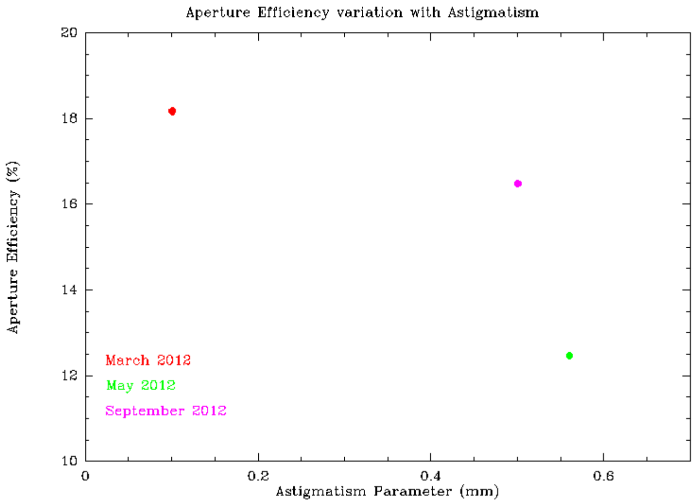

Figure 11: *Aperture efficiency variation with the astigmatism parameter for an elevation between 40° and 49°. The upper dot is for the March session and the lower one from May. September data appears in between, pointing to a surface accuracy recovery.*

6 Mirror Alignment

We investigated the possible degradation of the beam and the efficiency reduction due to a misalignment of the mirrors along the optical path. To do so, a laser was placed in the 87/22 GHz rail, as can be seen in figure 12. The laser radiation was reflected on two elliptical mirrors (M6 and M7), a planar mirror and a final elliptic mirror.

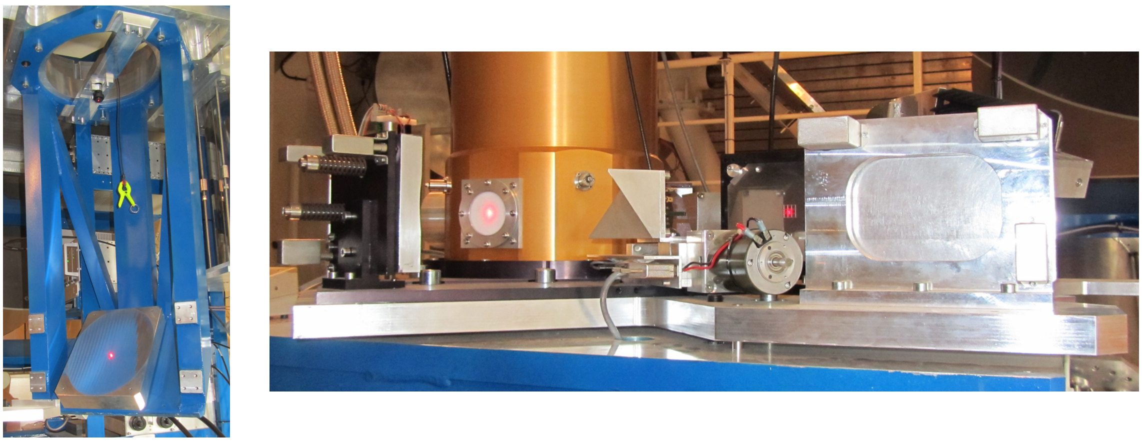

Figure 12: *Laser placed in the 22/87 GHz structure (left). Its light is reflected on the different mirrors along the optical path (right)*

All those mirrors are grooved with a grid that allows to see a red laser for alignment purposes. We moved mirror M6, which is fixed to the laser, along the rail, 5 mm away from its nominal position on both directions, to check the light reflections through the optical path. If every element of the optical system were in its best position, the light spot should stay at the center of the grid and the cryostat window.

According to figure 13 the current nominal position of the 3 mm receiver is not the optimum one. The spot is at the center of the grid on the first flat mirror, but it is not at the center of the cryostat window. As the laser was shifted from the optimum position 5 mm away in both directions, the light of the laser reflects on the flat mirror away from the center of the grid, changing sides as the laser goes through the optimum position. However at -5 mm, the laser illuminates the center of the cryostat window while at 0 and +5 mm the light is deflected towards the same direction and $\sim$3 mm away from the center. We believe that the 87 GHz may be laterally defocused. More tests are mandatory at the beginning of the next 87 GHz campaign to define the optimal position for the receiver.

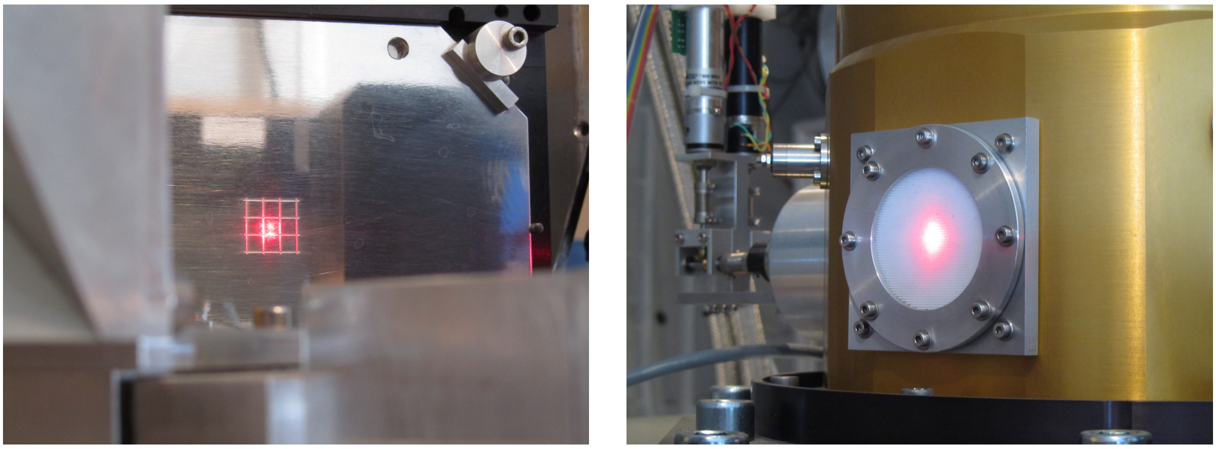

Figure 13: *Incidence area for the laser light on the first grid and the teflon cryostat window for the nominal position*

Diffraction effects were seen but the optical frequency is about 8 orders of magnitude higher than the receptor working frequency, so no diffraction pattern is expected at 87 GHz. The mechanization of the elliptical mirror left the surface with large scale facets, visible with the

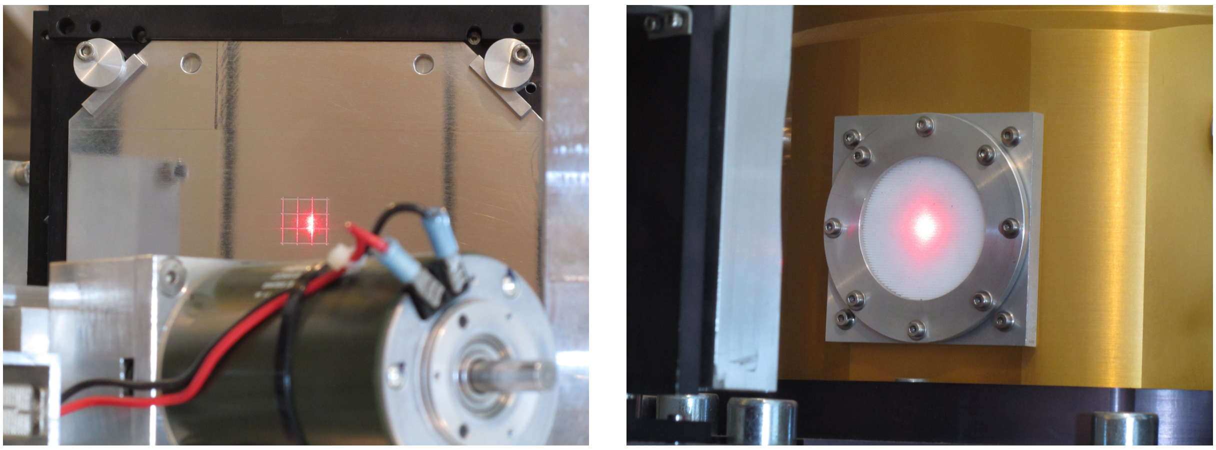

Figure 14: *Incidence area for the laser light on the first grid and the teflon cryostat window for 485 mm*

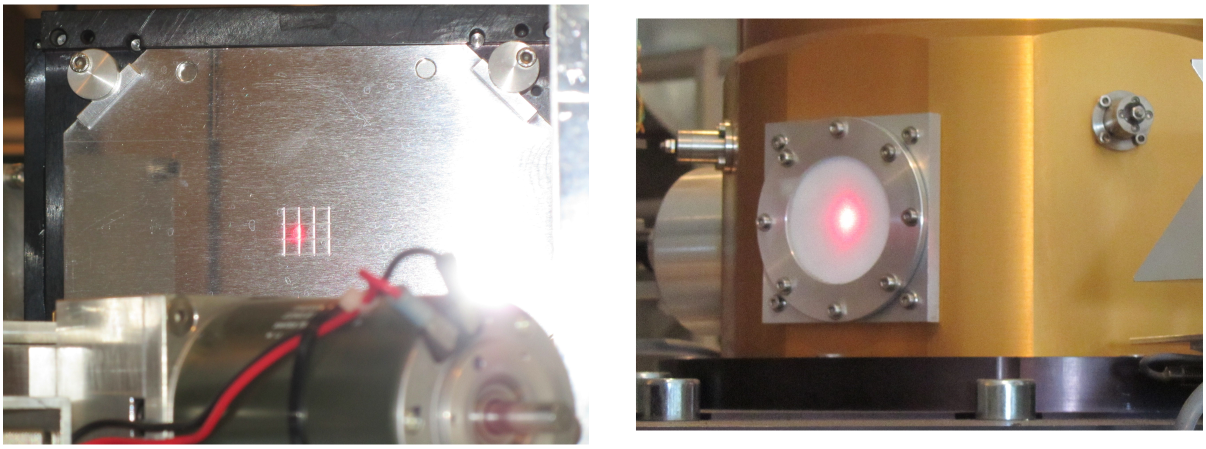

Figure 15: *Incidence area for the laser light on the first grid and the teflon cryostat window for 505 mm*

naked eye, which may degrade the beam reducing the efficiency but it was checked before its assembly in the optical path and its manufacture fulfilled all the requirements so its surface should be fine at 3 mm.

7 Astigmatism after holography

In order to check if the antenna has astigmatism, an holography session was scheduled in July 18-19 (López-Pérez, 2012 in preparation). Astigmatism was present in the first map. Several maps of 32x32 pixels were done along 24 hours to evaluate if temperature affects the deformation of the main reflector. The deformation was estimated to change from 1 mm during night-time to 2 mm during day-time.

8 Conclusions

- Lateral defocussing seems to be corrected: pointing drifts and OTF maps do not show apparent secondary lobes, so coma aberration has been reduced.
- Telescope pointing is good after the new pointing model: errors are below 10% of the beam.
- Since the pointing model was computed using the 22 GHz receiver an effort should be done to do it at 3 mm. This can be tested once pseudo-continuum observations are implemented in the telescope control software.
- The maximum efficiency of the antenna at 87 GHz has dropped from $\sim 28\%$ to $\sim 16\%$.
- The beam width is larger than expected. On the other hand the power drop due to axial defocussing is smaller than predicted. Both results indicate that possibly for the time being, there is no defined focus position, but a broad focusing area. It is not clear if this effect comes only from deformations on the primary reflector or also to a misplaced horn.

- The beam widening along orthogonal axis points to astigmatism in the primary reflector. This hypothesis was confirmed with holographic measurements.
- It may be possible that the antenna suffers seasonal deformations, with a strong dependence on temperature. This hypothesis should be checked with regular periodic observations together with holography sessions. If that were the case, the primary reflector surface should be adjusted from holography in winter time and 87 GHz observations should be restricted to winter, and preferably during night time.
- The position of the receiver is not the optimum. It is possible that the beam is deflected along the optical path and reaches the horn with some angle contributing to the signal degradation and the efficiency loss.

Further studies on the antenna at 3 mm are required. An optimum position for the receiver should be found which would imply a new focus and pointing model, posibly using pseudo-continuum observations. New gain curves should be obtained after to recalculate the aperture efficiency.

References

[de Vicente 2012] P. de Vicente "The 40m radiotelescope al the 87-110 GHz band after holography". IT-OAN 2012-09

[Lopez-Pérez 2012] J. A. López-Pérez, P. de Vicente "Analysis of the 40 meter radiotelescope beam and apperture efficiency at 100GHz from measured data" IT-OAN 2012-12

[de Vicente 2008] P. de Vicente "Preliminary characterization of the 40m radiotelescope at 22 GHz " IT-OAN 2008-8

[Baars 2007] J. W. M. Baars "The paraboloidal Reflector Antenna in Radioastronomy and Communication: Theory and Practice". Astrophysics and Space Science Library, vol.348, Springer 2007

[Albi 2012] T. Alonso, P. de Vicente, V. Bujarrabal "Implementation of the pointing model for the 40m OAN radiotelescope" IT-OAN 2010-3

[Davies 1970] J. H. Davies "The evolution of Reflector Antennas" Technical Report NGL-006-70-1, NASA, 1970.

[Greve 1994] A. Greve, B. LeFloch, D. Morris, H. Hein, S. Navarro "Astigmatism in Reflector Antennas: Measurement and Correction"